Journal of GeoEngineering, Vol. 14, No. 3, pp. 129-139, September 2019
http://dx.doi.org/10.6310/jog.201909_14(3).2

PENETRATION RESISTANCE OF JACK-UP SPUDCAN ON DENSE SAND OVERLYING LOOSE SAND

Yung-Show Fang [1*], Cheng Liu [2], Sheng-Lin Chen [3], and Ying-Chu Shih [4]

ABSTRACT

This paper presents experimental data associated with the penetration resistance of a conical spudcan penetrating a dense sand layer overlying loose sand. Saturated Ottawa sand was used as the seabed material. The instrumented 1-g physical model spudcan testing facility at National Chiao Tung University was used to investigate the variation of resistance profiles of a spudcan on a dense sand layer overlying a weaker stratum of loose sand. Based on the experimental data, it was found that the measured penetration resistance on the spudcan was in fairly good agreement with that estimated with the equations suggested by the Society of Naval Architects and Marine Engineers (2008). When the spudcan was extracted from the granular soil, the penetration resistance on the spudcan suddenly vanished. The upward moving spudcan was separated from soil particles below. For the spudcan penetrating a dense sand layer overlying loose sand, no peak penetration resistance and no abrupt post-peak softening was recorded, and no "punch-through" failure happened. The penetration profiles for a single dense sand layer and a single loose sand layer constituted the upper and lower bounds for the penetration curves for all different dense sand thickness conditions. At the critical void ratio, the backflow of soils induced a footprint sloping angle nearly equal to its residual internal friction angle, irrespective of its original density and shear strength.

Key words: Angle of repose, footprint, model test, sand, soil density, penetration resistance, spudcan.

1. INTRODUCTION

The potential for unexpected punch-through failure of a pack-up spudcan existed during installation in layered soils (Young *et al.* 1984). Such failure could lead to buckling of the jack-up leg, temporarily decommission the platform, and even toppling the unit (Lee *et al.* 2013). A compilation of reported incidents involving jack-up foundation incidents was summarized by Dier *et al.* (2004). It was concluded that one third of jack-up accidents had been associated with foundation problems. Punch-through had the highest rate in incidents, representing 53% of all foundation problems. Osborne and Paisley (2002) reported that spudcan punch-through failures occurred at an average rate of one incident per year, costing the industry between US$ 1 to 10 million per incident.

Lee *et al.* (2013) reported that when a jack-up spudcan was installed on seabed consisted of a sand layer overlying soft clay, the potential for "punch-through" failure existed. Based on their centrifuge tests, a typical penetration profile was illustrated in Fig. 1. In this case, the prototype spudcan diameter was 10.0 m and the sand thickness was 6.2 m. In the figure, the penetration profile consisted of a peak penetration resistance q_{peak}, near the sand surface, followed by an abrupt post-peak softening, and a reduction of 111 kPa was recorded between q_{peak} of 447 kPa and a $q_{post\text{-}peak}$ of 336 kPa.

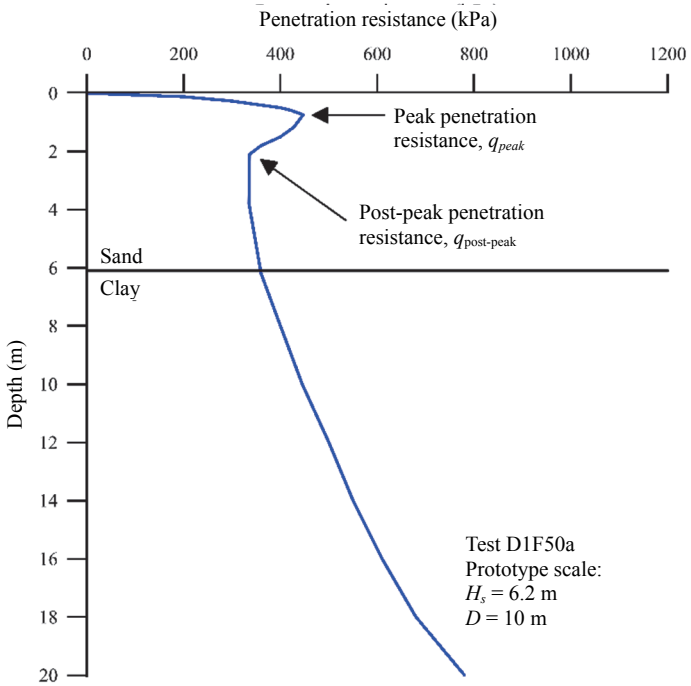

Fig. 1 Typical foundation penetration profile on sand overlying clay from centrifuge test (redrawn after Lee *et al.* 2013)

Manuscript received December 24, 2018; revised April 22, 2019; accepted April 26, 2019.
[1*] Professor (corresponding author), Department of Civil Engineering, National Chiao Tung University, Hsinchu, Taiwan 30010, R.O.C. (e-mail: ysfang@mail.nctu.edu.tw).
[2] Ph.D. Candidate, Department of Civil Engineering, National Chiao Tung University, Hsinchu, Taiwan 30010, R.O.C.
[3] Resident Engineer, Aerospace Industrial Development Corporation, Taichung, Taiwan 407, R.O.C.
[4] Graduate student, Department of Civil Engineering, National Chiao Tung University, Hsinchu, Taiwan 30010, R.O.C.

In the literature, soil conditions of a layer of sand overlying a weaker stratum of clay were widely studied. In this article, the soil condition of a layer of dense sand overlying a weaker stratum of loose sand was investigated. An example of offshore site where a dense sand layer overlying a weaker stratum of sand was introduced by Jardine *et al.* (1998). The authors investigated the axial capacity of offshore plies in dense North Sea sands. In the sedimentation process, the dense fine sand layer with a relative density D_r = 77% was overlying the medium dense fine sand with D_r = 63% at the AD II site of the Leman field. This study was intended to explore whether the unexpected punch-through failure, the abrupt reduction in bearing resistance would happen in an uncontrollable manner, when the spudcan was installed under such a soil condition. If not, what kind of penetration profile should be expected?

Taiwan is a small island with limited land and energy resources. The Bureau of Energy (2016) indicated that 97.95% of the energy consumed in Taiwan was imported. To reduce the negative environmental impacts due to the generation of energy from coal, fossil fuel, and nuclear materials, the government of Taiwan started the "Thousand Wind Turbine" project. Before the year 2025, the expected capacity from offshore wind power should reach 5.5 GW. At present, only two demonstration offshore wind turbines had been installed as shown in Fig. 2. These wind turbines were located at Formosa I wind farm off the west coast of Miaoli County. The two demonstration wind turbines with the capacity of 4 MW each were manufactured by Siemens and installed by Swancor (2017). The installation of these wind turbines and associated cables were completed on October 27 of 2016. The Changhua offshore wind farms subsurface investigation report by Taiwan Power Company (2009) indicated that the seabed sediments on the west coast of Taiwan included layers of silty clay (classified as CL and ML) and silty sand (classified as SM and SP) with different densities. As a result, the penetration resistance of the jack-up spudcan on layered soils became an important research subject.

This paper presents experimental data associated with the penetration resistance of a spudcan penetrating a dense sand layer overlying loose sand. Based on the test data, failure mechanisms of soils near the spudcan were proposed. All of the experiments mentioned in this paper were conducted in the National Chiao Tung University (NCTU) 1-g model spudcan testing facility, which was briefly described in the following sections. Saturated Ottawa sand was used as the seabed material. Penetration resistance on the spudcan was measured by a six-component force transducer. It was hoped that these test results would enhance a better understanding regarding the development of penetration resistance on the spudcan and the shape of footprint induced by the spudcan penetration and extraction.

Fig. 2 Offshore wind turbines at Formosa 1 wind farm in Taiwan (after Swancor 2017)

2. THEORETICAL SOLUTIONS

To justify the experimental findings of this study, test data obtained should be compared with existing theoretical solutions and design guidelines. The bearing capacity equations suggested by Meyerhof (1963) and the Society of Naval Architects and Marine Engineers (SNAME 2008) were summarized as follows.

2.1 Bearing Capacity Equation by Meyerhof

By considering the important factors (such as the foundation shape, depth, and load inclination) that influenced the bearing capacity q_u of a shallow foundation, Meyerhof (1963) suggested the following general bearing capacity equation:

$$q_u = c' N_c F_{cs} F_{cd} F_{ci} + q N_q F_{qs} F_{qd} F_{qi} + 0.5\,\gamma' B N_\gamma F_{\gamma s} F_{\gamma d} F_{\gamma i} \quad (1)$$

where c' = effective cohesion; q = effective overburden pressure at the level of the bottom of the foundation; γ' = effective unit weight of soil; B = width of foundation (= diameter for a circular foundation); F_{cs}, F_{qs}, $F_{\gamma s}$ = shape factors; F_{cd}, F_{qd}, $F_{\gamma d}$ = depth factors; F_{ci}, F_{qi}, $F_{\gamma i}$ = load inclination factors; N_c, N_q, N_γ = bearing capacity factors.

2.2 Penetration Resistance Equations by SNAME

In 2008, the Technical and Research Bulletin 5-5A relating to the site-specific assessment of mobile jack-up unit was published by SNAME. In Section C6.2.3 of the Bulletin, it was described that the ultimate vertical bearing capacity F_v of a circular footing resting in silica sand or other granular material could be computed by the following equation:

$$F_v = A\,(0.5\gamma' B N_\gamma s_\gamma d_\gamma + p_o' N_q s_q d_q) \quad (2)$$

where A = spudcan effective bearing area; p_o' = effective overburden pressure at the depth of bearing area; s_γ, s_q = shape factors; d_γ, d_q = depth factors. It should be noted that Eq. (2) was derived from Eq. (1). The first term on the right-hand-side of Eq. (1) vanished because the cohesion in silica sand was equal to zero. Since the applied loading was vertical, all load inclination factors were equal to 1. On the right-hand-side, the first term in Eq. (2) was the last term in Eq. (1), and the second term in Eq. (2) was the middle term in Eq. (1). At the end of Section C6 of SNAME (2008), the factors in Eq. (2) were defined as follows:

$$N_\gamma = 2(N_q + 1)\tan\phi \quad (3)$$

$$s_\gamma = 1 - 0.4\left(\frac{B}{L}\right) \quad \text{(0.6 for circular footing)} \quad (4)$$

$$d_\gamma = 1 \quad (5)$$

$$N_q = e^{\pi \tan\phi} \tan^2(45 + \phi/2) \quad (6)$$

$$s_q = 1 + \left(\frac{B}{L}\right) \tan\phi \quad (7)$$

$$d_q = 1 + 2\tan\phi\,(1-\sin\phi)^2\,(D/B) \quad (\text{for } D/B \le 1)$$
$$= 1 + 2\tan\phi\,(1-\sin\phi)^2 \tan^{-1}(D/B) \quad (\text{for } D/B > 1) \quad (8)$$

where ϕ = angle of internal friction for sand (degrees); B = effective spudcan diameter; L = foundation length (for circular foundation $L = B$); D = distance from mudline to spudcan maximum bearing area. In this study, the theoretical penetration resistance of the spudcan was calculated with the equations proposed by SNAME (2008). It should be mentioned that in this study, the diameter of spudcan was defined as D instead of B, and the depth of spudcan penetration was defined as z instead of D. The vertical force acting on the circular spudcan was defined as V_z instead of F_v.

3. NCTU MODEL SPUDCAN TESTING FACILITY

3.1 Vertical Loading System

The vertical loading system employed for this study could be divided into the following parts: (1) reaction frame; (2) axial force loading device; (3) speed control panel; (4) force transducer; and (5) displacement transducer as illustrated in Fig. 3.

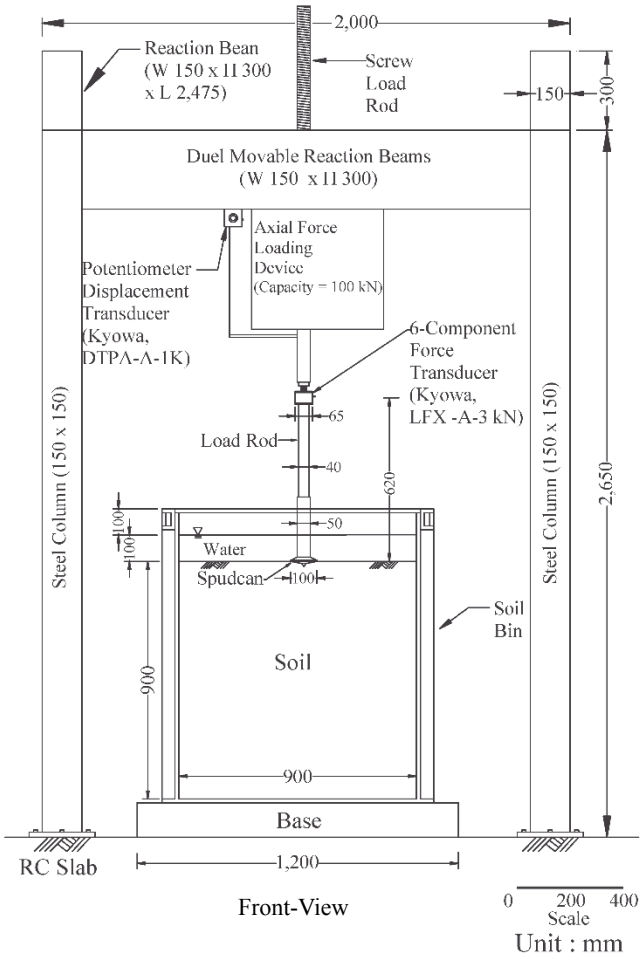

Fig. 3 Spudcan loading system with reaction frame

3.1.1 Reaction Frame

Above the soil bin, a steel reaction frame was constructed to resist the reaction force due to the penetration of spudcan into soils. As indicated in Fig. 3, the reaction frame was made of four 150 mm × 150 mm × 2,650 mm steel columns, two 150 mm × 300 mm × 2,475 mm horizontal steel H-beams, and two 150 mm × 300 mm × 2,000 mm movable horizontal steel beams.

3.1.2 Axial Force Loading Device

The motor-and-gear loading device indicated in Fig. 3 was used to push down and pull up the model spudcan in the vertical direction. The capacity of the loading machine was 100 kN, and its maximum stroke was ±450 mm.

3.1.3 Speed Control Panel

By adjusting the frequency of the alternating current supplied to the motor, this panel controlled the descending and ascending speed of the model spudcan. Martin and Houlsby (2000) conducted model tests with spudcan penetration speed of 0.33 mm/s. Hossain *et al.* (2006) conducted full and half model spudcan tests with the speeds of 0.20 mm/s and 0.05 mm/s. Following these laboratory studies, both upward and downward speeds of the model spudcan were controlled to 0.34 mm/s in this study.

3.1.4 Force Transducer

A 6-component force transducer (Kyowa, LFX-A-3kN) was used to measure the reaction force on the model spudcan during penetrating and uplifting. The transducer was capable of simultaneous measurement of 3 components of force (H_x, H_y, V_z) and 3 moments (M_x, M_y, M_z) acting on the spudcan. However, for this study only the vertical force V_z on the spudcan was measured. The capacity of vertical force for this load cell was 3 kN.

3.1.5 Displacement Transducer

A potentiometer-type displacement transducer (Kyowa, DTPA-A-1K) was used to measure the downward and upward displacement of the model spudcan. The rated capacity of this transducer was 1,000 mm. Before testing, a stainless steel wire was pulled out from the transducer to an extension rod connected to the load rod. With the penetration of spudcan into soil, the load rod moved down, and the wire was pulled out accordingly.

3.2 Soil Bin

It is important that the soil bin should be large enough so that the soil failure zone near the penetrating spudcan would not be confined by the rigid boundaries. Based on her centrifuge experiment results, Lu (2007) reported that for a spudcan with the diameter D = 6 m penetrated 5 m into seabed, the soils within $D/2$ on the sides and the depth D below the spudcan base were significantly disturbed. Test results reported by Hossain and Randolph (2010) indicated that for a spudcan with the diameter D = 6 m penetrated 6 m into clay, significant soil displacements were observed within 0.6D below the spudcan base. However, soil movements of both sides of the spudcan were not obvious.

In this study, the diameter of the model spudcan was 100

mm. Figure 4 showed the schematic diagram of the bin to contain the soil specimen. Its inside dimensions were 900 mm × 900 mm × 1,100 mm. In Fig. 3, the height of soil specimen and water were 900 mm and 1,000 mm, respectively. It was obvious that sufficient space was provided between the spudcan and surrounding boundaries. The 20 mm-thick steel sidewalls, steel base plate, twelve 38.5 mm × 38.5 mm box-type steel columns, and 16 steel beams were carefully welded together to ensure the stiffness of the bin. Since the soil specimen was fully submerged during testing, the 5 mm-thick inner wall was made of stainless steel to prevent rusting.

To simulate a saturated condition for seabed soils, after the laboratory specimen was submerged, the air remained in the soil sample was removed by suction. To achieve an air-tight chamber, a 1,060 mm-long, 1,060 mm-wide, and 25 mm-thick acrylic cover-plate was made. After the soil specimen was pluviated, and inundated in the bin, the cover plate was placed on top of the soil bin. Then air trapped in the submerged soil was sucked out by a vacuum pump.

3.3 Model Spudcan

The shape and dimensions of the conical model spudcan used for all experiments in this investigation was illustrated in Fig. 5. The spudcan was made of solid steel and had a diameter of 100 mm. In this study, the depth of penetration of the spudcan was defined for the amount of vertical displacement of the load reference point (L.R.P.) from the mudline shown in Fig. 5(a), and a picture of the model spudcan was shown in Fig. 5(b). The vertical reaction force, defined as V_z, acting on the spudcan was assumed to pass through the L.R.P. Figure 6 showed a picture including the movable reaction beam, loading device, force transducer, model spudcan, and soil bin of the NCTU model spudcan testing facility.

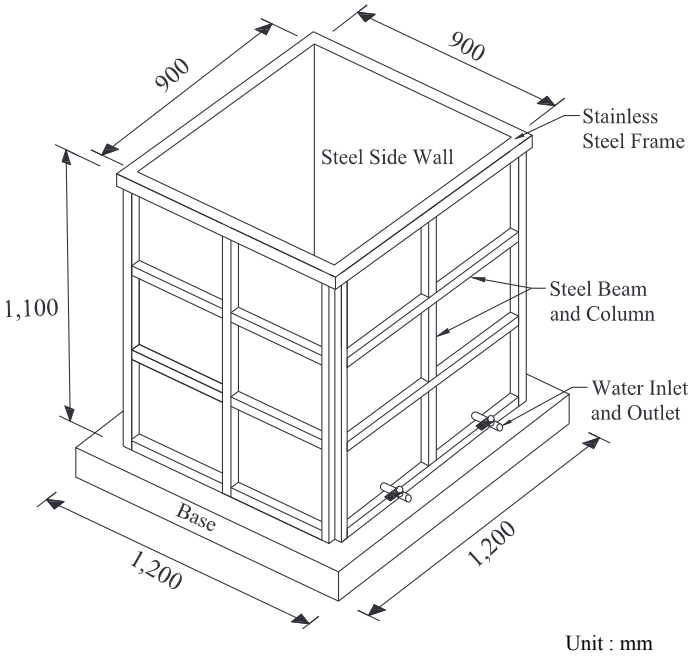

Fig. 4 Schematic diagram of soil bin

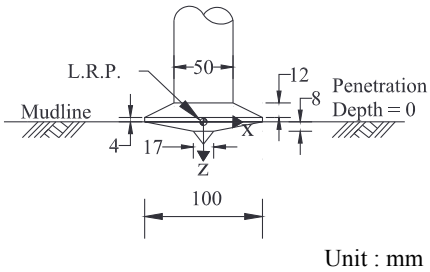

(a)

(b)

Fig. 5 Shape and dimensions of model spudcan

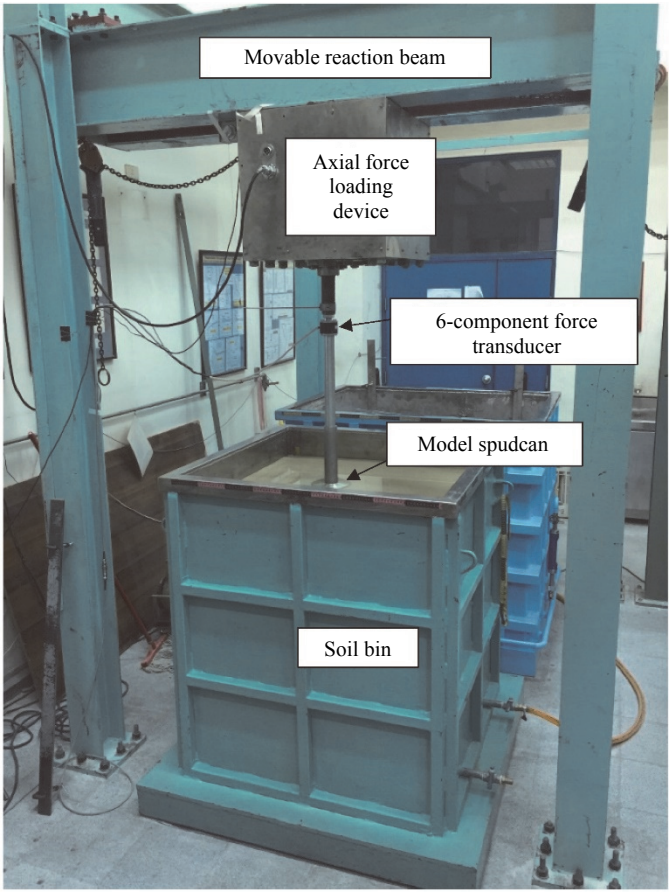

Fig. 6 NCTU model spudcan testing facility

3.4 Data Acquisition System

Due to the considerable amount of data collected during the test, a data acquisition system was used. For the 6-componant force transducer, a dynamic stain amplifier was built in the load cell. The output analog signal was collected and digitized by the data logger (GRAPHTEC, GL240). The digitized data was then transmitted to the computer to obtain the vertical force V_z on the spudcan. For the potentiometer-type displacement transducer, the analog signal from the sensor was filtered and amplified by the dynamic strain amplifier (Kyowa, DPM-711B), then digitized by an analog-to-digital converter. The digitized signal was then transmitted to the computer for storage and analysis.

4. SPECIMEN PREPARATION AND TEST PROCEDURE

Ottawa sand was used for all model experiments in this study. Physical properties of the soil included G_s = 2.65, e_{max} = 0.76, e_{min} = 0.50, D_{60} = 0.39 mm, and D_{10} = 0.26 mm. The Ottawa sand was classified as SP by the Unified Soil Classification System.

4.1 Specimen Preparation

To achieve the desired dry soil densities of 17.3%, 36.5%, 51.2%, 69.3%, and 83.5%, air-dry Ottawa sand was deposited by air-pluviation from the slit of a hopper into the soil bin. To obtain the initial relative density of 17.3%, the slot opening of the hopper was 10 mm, and the drop distance was approximately 0.2 m from the soil surface throughout the placement process. The air-pluviation method had been widely used to reconstitute sand samples in the laboratory. Rad and Tumay (1987) reported that pluviation method provides reasonably homogeneous specimens with desired relative density. Lo Presti *et al.* (1992) concluded that the pluviation method is an efficient way of preparing large soil sample. Density control molds were used to evaluate the variation of soil density in the soil specimen. The cylindrical mold was made of acrylic with an inner diameter of 152.4 mm and a height of 155.2 mm (ASTM D4254 2014). For the density distribution experiment, the molds were buried in the soil mass. After the entire specimen had been placed, the molds were extracted and the unit weight of soil in the mold was determined. It was found that the soil density was relatively uniform in the soil mass.

Chen (1997) reported that the air-pluviated soil density increased with increasing drop distance and decreasing slot opening. To achieve the dense condition, the slot opening of the hopper was 5 mm, and the drop distance was approximately 1.2 m. The achieved relative density in the soil specimen was about 69.3%. The measured water content of air-dry Ottawa sand used was 0.12%. As indicated in Fig. 3, typical specimen size for all experiments in this study was 900 mm × 900 mm × 900 mm.

4.2 Volume Reduction Due to Submergence and Suction

To simulate the behavior of seabed soils, the Ottawa sand specimen should be saturated. Das and Sobhan (2018) suggested that for granular soil deposits, the relative density D_r between 15% and 50% was described as loose, the D_r between 50% and 70% was defined as medium, and the D_r between 70% and 85% was described as dense. For a loose soil specimen shown in Fig. 7, the initial relative density was 17.3%. After soil placement, water flowed into the soil bin, until the water surface rose to 100 mm above soil surface as illustrated in Fig. 3. After inundation, the relative density of soil increased significantly (+8.0%) to 25.3%. To remove the air trapped among soil particles, an air-tight cover plate was attached to the top of the soil bin, then a suction of −50 kPa was applied by a vacuum pump for 8 hours. After suction, the relative density of soil rose slightly (+0.8%) to 26.1%. Since the cubic soil specimen had a constant cross-section area, the reduction of soil volume was obtained by measuring the decrease of specimen height. The measured volume-weight relationship of the flooded and sucked specimen indicated that the degree of saturation achieved was 100%.

For the dense specimen shown in Fig. 7, the initial relative density was 69.3%. After flooding, the relative density of soil increased only slightly (+1.2%) to 70.5%. After suction, the relative density of soil rose slightly (+0.9%) to 71.4%. In Fig. 7, a series of tests were conducted for the cohesionless soil with five initial densities. It could be concluded from these data that, for a loose specimen, the volume reduction due to submergence was much greater than that due to suction. However, this volume reduction due to inundation decreased with increasing soil density. For a dense soil specimen, since the soil particles were initially densely packed, neither the flooding nor suction could cause the soil skeleton to compress significantly.

4.3 Test Procedure

After the submerged soil specimen was properly prepared, the axial force loading device and the movable reaction beam was moved to the location of spudcan penetration as indicated in Fig. 6. A horizontal L-shaped steel beam was placed on top of the soil bin, and a digital vernier caliper was used to measure the elevation profile of soil surface before testing. Then the model spudcan was carefully attached to the loading rod. In Fig. 8 (a),

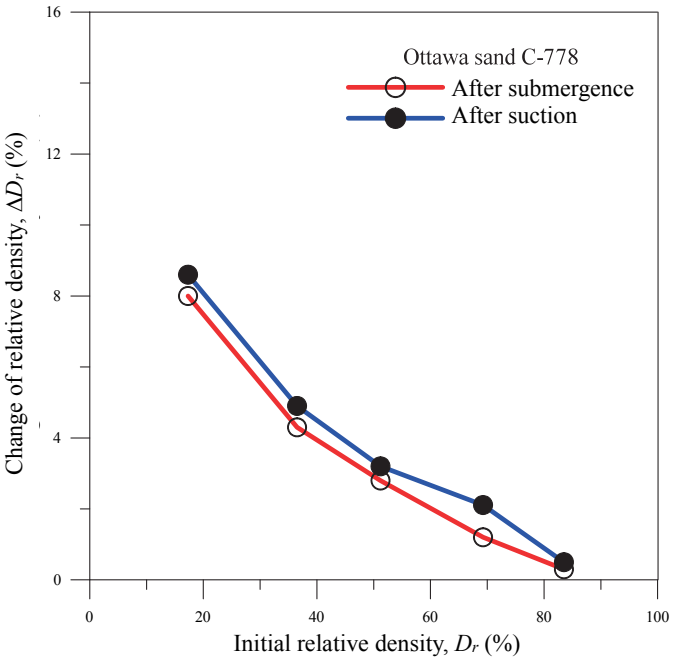

Fig. 7 Relative density change due to submergence and suction

the axial loading device pushed the submerged spudcan downward, slowly approaching the mudline at the speed of 0.34 mm/s.

It should be mentioned again that in this article, the penetration depth z was defined as the amount of penetration of the L.R.P. Figure 8(b) showed, as the L.R.P. reached the mudline, the penetration depth was equal to zero. Figure 8(c) showed that when the desired penetration depth 350 mm was reached, the penetration stopped, and a depression cone of soils was formed around the loading rod.

Then the spudcan was retracted from the disturbed soils at the speed of 0.34 mm/s. After the spudcan was totally pulled out, the footprint profile (shown in Fig. 8(d)) due to the spudcan penetration and extraction was measured.

5. TEST RESULTS

This section reports the testing procedure and experimental results regarding the penetration resistance on a spudcan on granular soil deposits.

5.1 Spudcan on Loose Sand

At the beginning of this study, a bench-mark experiment test was conducted to investigate the vertical force on the spudcan penetrating a horizontal loose seabed. The diameter D of the circular spudcan was 100 mm. The unit weight of the loose saturated specimen was 19.37 kN/m^3, and its relative density was 26%. Based on direct shear test results, the corresponding internal friction angle of the loose sand was 31.7°. The purple curve in Fig. 9 showed the variation of vertical force V_z on the spudcan with normalized penetration depth z/D. Before the spudcan touched the seabed, the measured vertical force was equal to zero. As the sharp bottom cone penetrated the soil surface, a tiny amount of resistance was recorded. As the L.R.P. reached the mudline (z = 0), the base cone of the spudcan was embedded in soils as illustrated in Fig. 5(a), and a certain amount of penetration resistance was measured. Test results in Fig. 9 clearly indicated that the penetration resistance increased with increasing depth of penetration.

After the projected penetration depth z = 350 mm had been reached, the penetration stopped and the spudcan was extracted from soils. It could be observed in Fig. 9 that since there was no adhesion between the metal spudcan and soil particles, the penetration resistance on the spudcan suddenly vanished. The upward moving spudcan was separated from discrete soil particles below. It should be noted in Fig. 9 that a small amount of suction on the spudcan was measured due to the unloading of the spudcan. However, because of the high permeability and effective drainage of the granular soil, the suction stress quickly dissipated. From a practical point of view, the vertical force on the spudcan throughout the extraction process could be considered as zero. It should be mentioned that during the extraction process, there existed a downward vertical force on the spudcan due to the self-weight of the sand above the flange of spudcan. However, since the area of the conical model spudcan was only 0.00785 m^2, and the depth of overburden was less than 350 mm, when compared to the significant bearing capacity in sand, the downward overburden force became negligible.

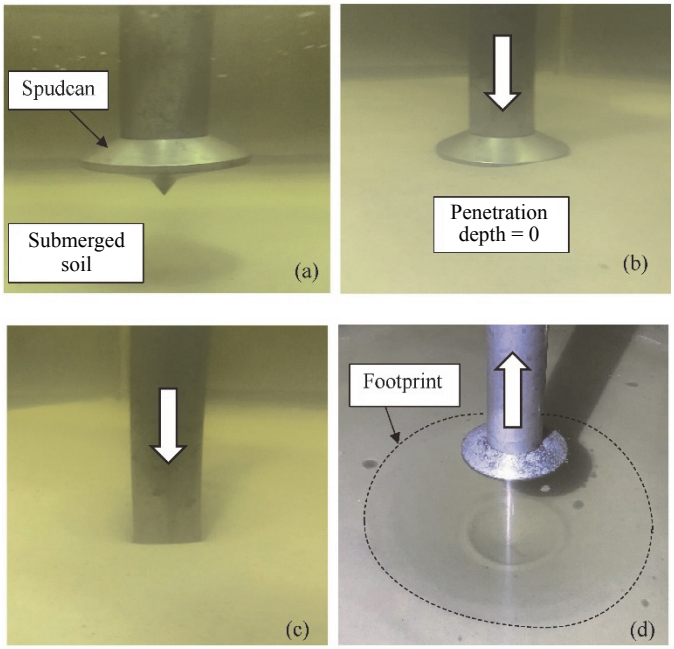

Fig. 8 (a) Spudcan approaching soil surface; (b) Spudcan start to penetrate (z = 0); (c) Spudcan penetrating submerged soils; (d) Extracted spudcan and footprint

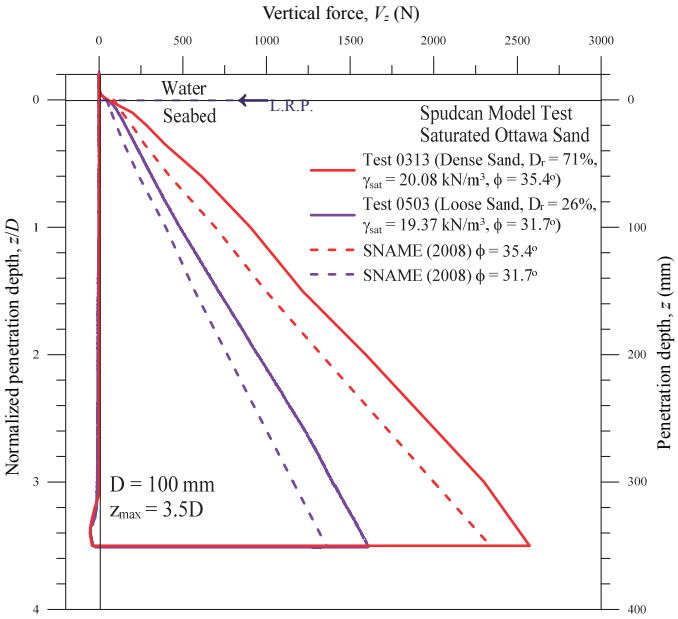

Fig. 9 Typical spudcan penetration profiles on pure loose and dense sand

5.2 Spudcan on Dense Sand

Another bench-mark experiment was conducted to investigate the penetration resistance on the spudcan penetrating a dense sand specimen. The unit weight of the saturated dense sand was 20.08 kN/m^3, and its relative density was 71%, with an internal friction angle of 35.4°. The red curve in Fig. 9 illustrated the rise of penetration resistance on the spudcan with increasing penetration depth. It was obvious that since the dense sand had a higher shear strength, the measured penetration resistance in dense sand

was greater than that measured in loose sand.

For comparison purposes, the vertical forces on the spudcan calculated with equations suggested by SNAME (2008) were also plotted with dashed curves in Fig. 9. Considering the assumptions made for the theoretical solution and model test details involved, it was concluded that the measured penetration resistance on the spudcan was in fairly good agreement with those estimated with the equations suggested by SNAME (2008).

5.3 Spudcan on Dense Sand Overlying Loose Sand

This section investigated the penetration resistance of the model spudcan on a dense sand layer overlying a weaker stratum of loose sand as indicated in Fig. 10. It was intended to explore, under this condition, whether the "punch-through" failure would happen to the spudcan or not. In Fig. 10, the thickness of the dense sand layer was defined as H_d. The total height H of the soil specimen in the soil bin was 900 mm. The thickness of the dense sand layer used for laboratory tests included 0, 50, 100, 200, 400, and 900 mm. The diameter of the conical spudcan was 100 mm.

Figure 11 showed the penetration resistance profiles obtained for tests with five different dense sand thickness. In Fig. 11, the test data for H_d/D = 0 was actually the loading curve for the spudcan penetrating loose sand. The test curve for H_d = 9.0 was the vertical resistance profile for the spudcan penetrating dense sand. For the green penetration profile with H_d/D = 1.0 in Fig. 11, initially the vertical force on the spudcan was almost identical to the penetration resistance obtained on dense soil. This phenomenon could be explained with the help of Fig. 12(a) based on Terzaghi (1943). In this H_d/D = 1.0 condition, the general shear failure surface under the spudcan was developed mostly in the dense sand layer. Therefore, it was reasonable to expect the measured initial penetration resistance to be almost identical to that obtained on a spudcan penetrating dense sand.

With the depth of penetration increased to 0.5D, 1.0D, and 2.0D, the measured penetration resistance data gradually deviated from the penetration curve for dense sand. Eventually, at the penetration depth z = 3.5D, the measured penetration profile converged to that for a spudcan penetrating loose sand. This phenomenon could be explained with the help of Fig. 12(b) based on Vesic (1967). In the figure, the failure surface caused by the spudcan penetration was quite similar to the end-bearing failure surface of a pile, which was developed mostly in loose sand. This was the reason why the vertical force measured at z = 3.5D was almost identical to the resistance force V_z measured on the spudcan on loose sand.

Lee *et al.* (2013) reported that when a jack-up spudcan was installed on seabed consisted of a sand layer overlying soft clay, the potential for "punch-through" failure existed. In Fig. 1, the penetration profile consisted of a peak penetration resistance, followed by an abrupt post-peak softening. In Fig. 11, the spudcan was installed on seabed consisted of a dense sand layer overlying a weaker stratum of loose sand. For H_d/D = 2.0, a change of curvature was observed on the yellow curve at the depth of H_d/D = 1.0 (z = 100 mm). With increasing depth of penetration, the curvature slowly decreased. However, no peak penetration resistance and no reduction of penetration resistance was recorded on the penetration profile. For all curves in Fig. 11, no peak penetration resistance and no abrupt post-peak softening was recorded. It could be concluded that since the loose sand was not really soft, no "punch-through" failure shown in Fig. 1 happened. In Fig. 11, the penetration profiles for dense sand and loose sand constituted the upper and lower bounds for penetration profiles for all dense sand thickness conditions.

Comparing Fig. 11 with Fig. 1, it was clear that in Fig. 11 there were no abrupt reduction of vertical force. The discrepancy in these two figures was most probably due to the different shear strength mechanism of the underlying sand and clay layers under large deformation. Holtz *et al.* (2011) stated that in the United States, the clay with a sensitivity of 4 to 8 is defined as "medium sensitive". This means that as the failure surface below the model spudcan cut through the underlying clay layer, the residual shear strength of clay could be reduced to only 12.5% to 25% of its undisturbed shear strength. This is probably the reason why there was an abrupt reduction in penetration resistance in Fig. 1.

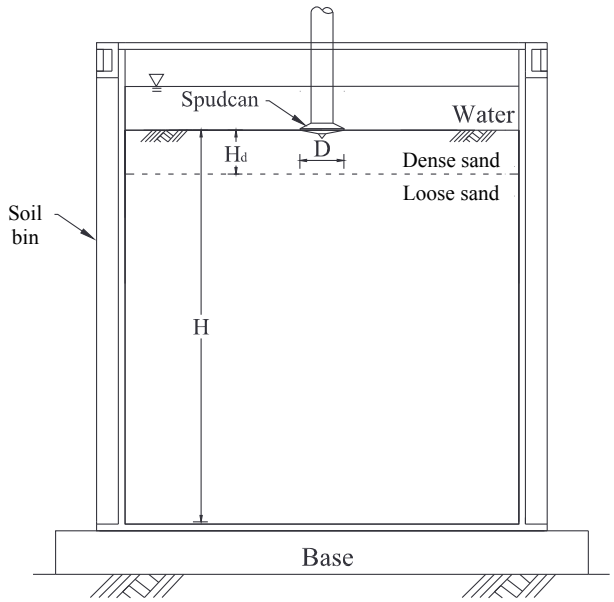

Fig. 10 Spudcan on dense sand overlaying loose sand

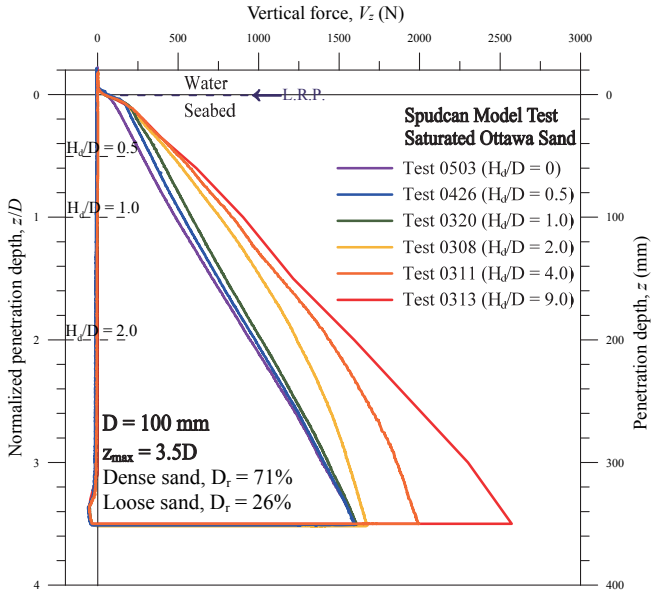

Fig. 11 Comparison of vertical resistance on spudcan penetration different thickness of dense sand overlaying loose sand

However, for the underlying loose sand in Figs. 12(a) and 12(b), the shear strength reduction due to increasing shear strain was less significant. Assuming the void ratio of the loose sand was nearly equal to its critical void ratio. After experiencing the large shear deformation due to spudcan penetration, the residual internal friction angle ϕ_r of sand would be nearly identical to its undisturbed ϕ angle. This is probably the reason why the vertical force curves in Fig. 11 were relatively smooth. These penetration resistance curves mainly reflected the relative densities and shear strength of the dense and loose sand strata.

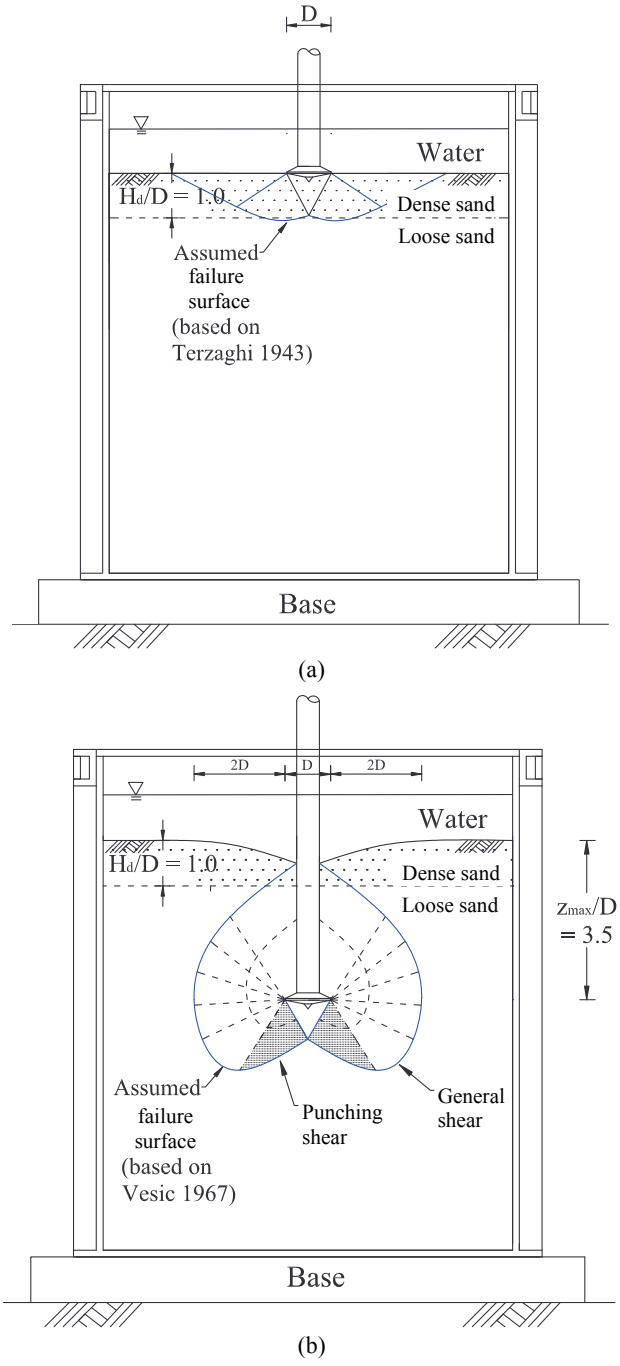

Fig. 12 (a) Proposed general shear failure due to spudcan penetrating surface dense sand layer based on Terzaghi (1943); (b) proposed punching and general shear failure due to spudcan penetrating deeper loose sand based on Vesic (1967)

Osborne *et al.* (2011) reported that for a spudcan penetration soft to firm clay or loose silt seabed, the amount of penetration could reach 0.5*D* to 2.0*D*. However, for a spudcan penetration seabed with uniform sand, the amount of penetration would be minimal. For this study, the sandy seabed was pretty stiff and strong. Depending on the loads on the jack-up unit and size of the spudcan, the actual depth of penetration in the field could be controlled to be less than 0.5*D*, which was significantly less than the maximum depth $z_{max} = 3.5D$ used for the model experiments in this study.

5.4 Footprints

This section discussed the settlement and sloping angle of the footprint left on the seabed surface due to the penetration and extraction of the spudcan. The distribution of settlement on the seabed surface at the xz and yz sections for five different dense sand thickness conditions were shown in Figs. 13(a) and 13(b). For Test 0503 ($H_d/D = 0$), the soil bin was filled with loose sand. The loose soils contracted due to vertical loading and associated shearing. Therefore the footprint settlements were the greatest among five sets of data. For Test 0313 ($H_d/D = 9.0$), the soil bin was filled with dense sand. As a result, the measured settlements were the smallest in Figs. 13(a) and 13(b). The volume of dense sand would contract and then dilate upon shearing. It was not surprising to observe some heaving of seabed on both sides of the footprint in Figs. 13(a) and 13(b).

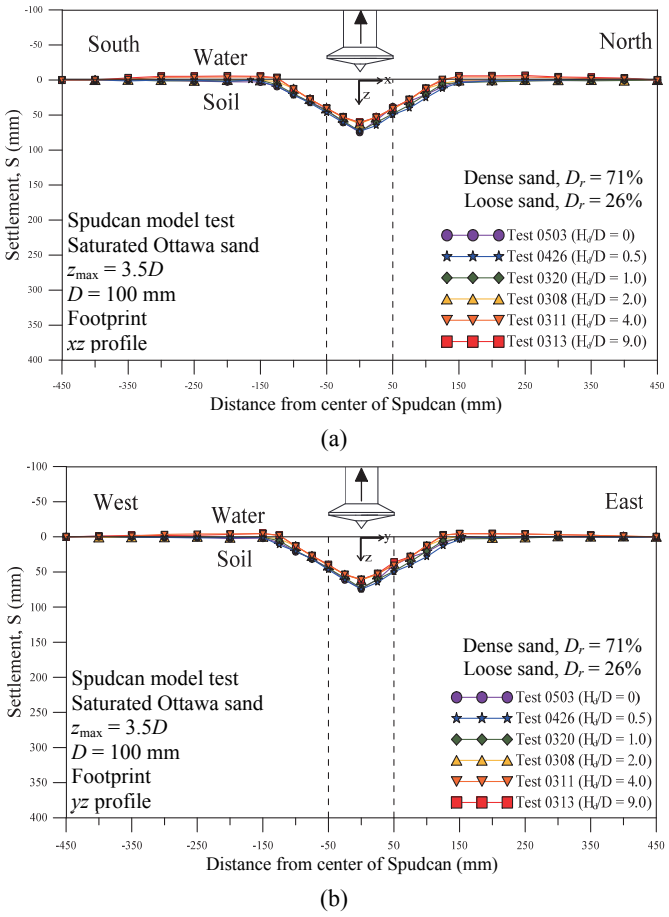

Fig. 13 Footprints caused by spudcan penetrating into seabeds with different H_d/D

5.4.1 Footprint Sloping Angle

Holtz and Kovacs (1981) described that when loose sand was sheared in a triaxial test, the principal stress difference ($\sigma_1 - \sigma_3$) gradually increased to an ultimate value. Concurrently, the volume of the specimen decreased from e_l (loose) down to a value very close to the critical void ratio e_{crit}. This condition was referred to as the ultimate, constant volume, or residual condition (Lambe and Whitman 1969). When a dense specimen was sheared, the principal stress difference reached a peak value and subsequently decreased to a value very close to $(\sigma_1 - \sigma_3)_{ult}$ for loose sand. The dense sand contracted slightly at first, then dilated up to a value very close to e_{crit}. It was clear that as dense sand dilated with increasing strain, the dense specimen was no longer "dense".

A typical experimental footprint profile was illustrated in Fig. 14. For a granular seabed, test data indicated that the main inclined surface of the footprint could be approximated with a cone. Linear regression analysis was carried out for points D to I in Fig 14, and the footprint sloping angle was found to be i = 30.3°. For points I to N in the figure, the footprint inclination angle was also i = 30.3°. This phenomenon could be explained with the concept of the repose angle of granular soils. When the spudcan was pulled out of seabed, a transient cylindrical space was generated by the upward movement of the circular spudcan as indicated in Fig. 14. When the spudcan moved up, the cylindrical cavity generated below the spudcan was instantly filled by the backflow of adjacent soil particles. On the conical footprint, the backflow particles formed an angle of repose i = 30.3°, which was quite close to the residual friction angle of Ottawa sand ϕ_r = 31.7° obtained from direct shear tests. It should be mentioned that in Fig. 14 points A to D, and N to Q on the depression curve were out of the cut of the infinite slope from point I. Therefore, these points did not backflow.

Figure 15 summarized the footprint sloping angles based on the regression analysis for test data measured at four directions (east, south, west, and north), at six different dense sand thickness (H_d/D = 0, 0.5, 1.0, 2.0, 4.0, and 9.0). The coefficient of determination R^2 for the regression analysis for 24 sets of data varied from 0.973 to 0.999. It was interesting to find that the range of footprint sloping angles (i = 29.8° to 31.3°) were fairly close to the residual internal friction angle of Ottawa sand (ϕ_r = 31.7°). Based on the critical state concept, when the soil was

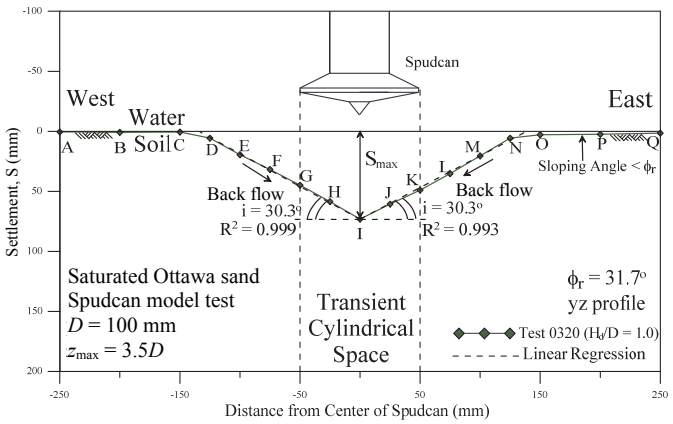

Fig. 14 Experimental footprint profile and its linear regression

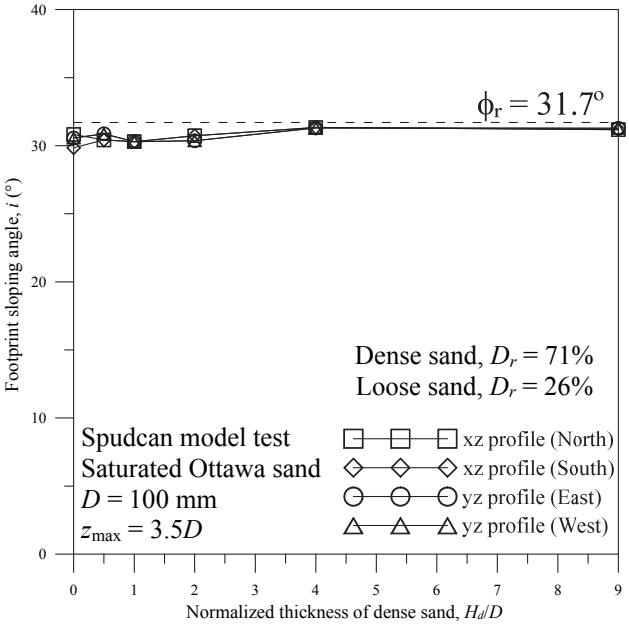

Fig. 15 Variation of footprint sloping angle with thickness of dense sand

severely sheared, and the soil would reach a critical state. At the critical void ratio, the backflow of soils induced a footprint sloping angle nearly equal to its residual internal friction angle, irrespective of its original density and shear strength.

It should be mentioned that, in this study the penetration depth of spudcan was 3.5D, and the seabed soils along the spudcan path were significantly sheared. If the depth of penetration was too small to remold adjacent soils, the footprint sloping angle might not be identical to the residual friction angle of soil.

5.4.2 Maximum Settlement

Figure 16 showed the variation of maximum settlement S_{max} (defined in Fig. 14) of the footprint, as a function of the thickness

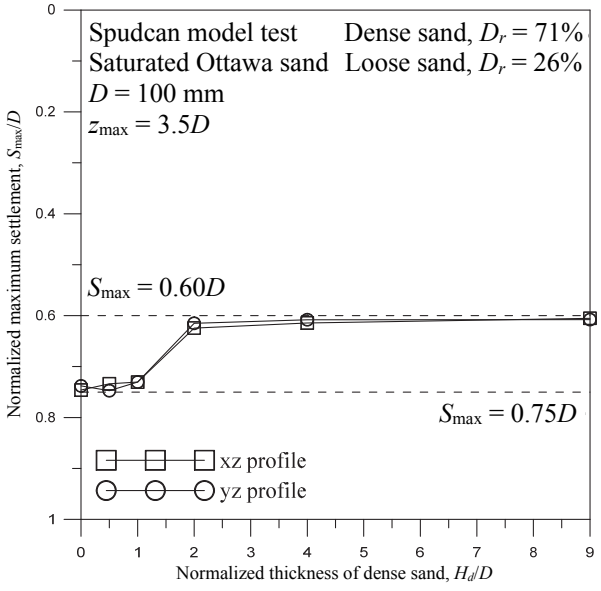

Fig. 16 Variation of maximum settlement with thickness of dense sand

of the dense sand layer. In the figure, the maximum settlement changed from 0.60D to 0.75D. For the spudcan on loose sand (H_d/D = 0), the soil specimen contracted the most under vertical load and shearing. Therefore the measured S_{max} was the largest. For the spudcan on dense sand (H_d/D = 9.0), the measured S_{max} was the smallest. The entire footprint crater was created by the downward compression of the spudcan. It should be noted that among many other factors, the maximum settlement was affected by the depth of penetration, spudcan diameter, and density of soil. It was apparent that more investigation regarding this subject was needed.

5.5 Limitations

In this study, the major limitation of the findings obtained from the 1-g physical model tests was the scale effect. For example, the area of the spudcan of the turbine installation vessel named "Torben" which built the offshore wind turbines shown in Fig. 2 was 90 m^2. Assuming that the spudcan was circular, the corresponding diameter of the spudcan would be 10.7 m, which was 107 times the diameter (D = 0.1 m) for the model spudcan. The minute stress and strain due to the spudcan penetration in the 1-g physical model could not fully simulate the stress and strain of the soil in the field. It should be emphasized that in this study, no quantitative finding was attempted, only primitive and qualitative observations regarding the failure mechanism and related soil behavior were reported. Scale effects of shallow foundation bearing capacity on granular materials were investigates to evaluate the trend of decreasing bearing capacity factor N_γ, with increasing footing width by Cerato and Lutenegger (2007). Results of the model-scale footing tests showed that the bearing capacity factor N_γ was dependent on the width of the footing for both square and circular footings. It was found that behavior of most model-scale footing test cannot be directly correlated to the behavior of full-scale tests because of differences in mean stresses experienced beneath footings of various sizes. It is obvious that more investigation based on centrifuge experiments, numerical studies, and full-scale tests associated with this subject are needed.

Other limitations of this study included that only a granular and horizontal seabed was considered. Only the vertical penetration loading was applied, so the horizontal force and bending moment due to ocean current, wind load, and earthquake excitation were neglected.

6. CONCLUSIONS

Based on the experimental data obtained during this investigation, the following conclusions could be drawn.

For air-dry loose sand, its volume reduction due to submergence was much greater than that due to the following suction. However, this volume reduction due to inundation decreased with increasing initial soil density. For a dense sand specimen, since the soil particles were initially densely packed, neither the inundation nor the following suction could cause the soil skeleton to compress significantly.

For a spudcan penetrating loose sand, the penetration resistance increased with increasing depth of penetration. When the spudcan was extracted from the granular soil, the penetration resistance on the spudcan suddenly vanished. The upward moving spudcan was separated from soil particles below. A small amount of suction on the spudcan was measured due to the unloading of the spudcan. However, the suction stress quickly dissipated. From a practical point of view, the vertical force on the spudcan throughout the extraction process could be neglected.

The measured penetration resistance in dense sand was greater than that measured in loose sand. The measured penetration resistance on the spudcan was in fairly good agreement with that estimated with the equations suggested by SNAME (2008).

For the spudcan penetrating the seabed consisted of a dense sand layer overlying a weaker stratum of loose sand, no peak penetration resistance and no abrupt post-peak softening was recorded. It was concluded that since the loose sand was not really soft, no "punch-through" failure happened. The penetration profiles for dense sand and loose sand constituted the upper and lower bounds for the penetration curves for all dense sand thickness conditions.

When the spudcan moved up, the transient cylindrical cavity generated below the spudcan was instantly filled by the backflow of adjacent particles. On the conical footprint, the backflow of granular particles formed a repose angle, which was quite close to the residual friction angle of Ottawa sand.

Based on the critical state concept, when the soil was severely sheared, the soil had reached a critical state. At the critical void ratio, the backflow of granular particles induced a footprint sloping angle nearly equal to its residual internal friction angle, irrespective of its original density and shear strength.

ACKNOWLEDGMENTS

The writers wish to acknowledge the Ministry of Science and Technology of Taiwan (R.O.C.) (MOST 105-2623-E-009-001-ET) for the financial assistance that made this investigation possible.

REFERENCES

ASTM International (2014). *ASTM D4254-91*, *Standard Test Method for Minimum Index Density and Unit Weight of Soils and Calculation of Relative Density*. West Conshohocken, PA, U.S.A. https://standards.globalspec.com/std/9996935/ASTM%20D4254

Bureau of Energy (2016). *2016 Annual Report of the Bureau of Energy*, Ministry of Economic Affairs, Taipei, Taiwan (in Chinese). https://www.moeaboe.gov.tw/ECW/populace/content/ContentLink.aspx?menu_id=137&sub_menu_id=358

Cerato, A.B. and Lutenegger, A.J. (2007). "Scale effects of shallow foundation bearing capacity on granular material." *Journal of Geotechnical and Geoenvironmental Engineering*, ASCE, 133(10), 1192-1202. https://doi.org/10.1061/(ASCE)1090-0241(2007)133:10(1192)

Chen, H.R. (1997). *Earth Pressure At-Rest with Different Soil Densities and Backfill Inclinations*. Master thesis, Department of Civil Engineering, National Chiao Tung University, Hsinchu, Taiwan. https://ir.nctu.edu.tw/handle/11536/61426?locale=zh_TWqs=chrome..69i57j69i58.747j0j4&sourceid=chrome&ie=UTF-8

Das, B.M. and Sobhan, K. (2018). *Principle of Foundation Engineering,* 9th Ed., Cengage Learning, Boston, U.S.A. https://www.cengage.com/c/principles-of-geotechnical-engineering-9e-das

Dier, A., Carroll, B., and Abolfathi, S. (2004). *Guidelines for Jack-Up Rigs with Particular Reference to Foundation Integrity*. Research Report 289, Health and Safety Executive (HSE), Bootle, U.K. http://www.hse.gov.uk/research/rrpdf/rr289.pdf

Holtz, R.D. and Kovacs, W.D. (1981). *An Introduction to Geotechnical Engineering*, Prentice-Hall, Inc., Englewood Cliff, New Jersey. http://worldcat.org/isbn/0134843940

Holtz, R.D., Kovacs, W.D., and Sheahan, T.C. (2011). *An Introduction to Geotechnical Engineering,* 2nd Ed., Pearson Education Inc., Upper Saddle. River, NJ, USA. https://www.pearson.com/us/higher-education/program/Holtz-Introduction-to-Geotechnical-Engineering-An-2nd-Edition/PGM151874.html

Hossain, M.S., Randolph, M.F., Hu, Y., and White, D.J. (2006). "Cavity stability and bearing capacity of spudcan foundations on clay." *Proceedings of the Offshore Technology Conference,* OTC 17770, Houston, Texas, U.S.A., 1-18. https://doi.org/10.4043/17770-MS

Hossain, M.S. and Randolph, M.F. (2010). "Deep-penetrating spudcan foundations on layered clays: Centrifuge tests." *Geotechnique*, **60**(3), 157-170. https://doi.org/10.1680/geot.2011.61.1.85

Jardine, R.J., Overy, R.F., and Chow, F.C. (1998). "Axial capacity of offshore piles in dense North Sea sands." *Journal of Geotechnical and Geoenvironmental Engineering*, ASCE, **124**(2), 171-178. https://doi.org/10.1061/(ASCE)1090-0241(1998)124:2(171)

Lambe, T.W. and Whitman, R.V. (1969). *Soil Mechanics*, John Wiley & Sons, Inc., New York, U.S.A. https://trove.nla.gov.au/version/45228333

Lee, K.K., Cassidy, M.J., and Randolph, M.F. (2013). "Bearing capacity on sand overlying clay soils: Experimental and finite element investigation of potential punch-through failure." *Geotechnique*, **63**(15), 1271-1284. https://www.icevirtuallibrary.com/doi/10.1680/geot.12.P.175

Lo Presti, D.C.F., Pedroni, S., and Crippa, V. (1992). "Maximum dry density of cohesionless soils by pluviation and by ASTM D4253-83: A comparative study." *Geotechnical Testing Journal,* **15**(2), 180-189. https://doi.org/10.1520/GTJ10239J

Lu, T.K. (2007). *Punch-Through of Spudcan Foundation in Sand Overlying Clay.* Ph.D. Dissertation, Department of Civil Engineering, National University of Singapore, Singapore. http://scholarbank.nus.edu.sg/handle/10635/28149

Martine, C.M. and Houlsby, G.T. (2000). "Combined loading of spudcan foundations on clay: Laboratory tests." *Geotechnique*, **50**(4), 325-338. https://doi.org/10.1680/geot.2000.50.4.325

Meyerhof, G.G. (1963). "Some recent research on the bearing capacity of foundations." *Canadian Geotechnical Journal*, **1**, 16-26. https://doi.org/10.1139/t63-003

Osborne, J.J., Teh, K.L., Houlsby, G.T., Cassidy, M.J., Bienen, B., and Leung, C.F. (2011). *Improved Guidelines for the Prediction of Geotechnical Performance of Spudcan Foundations during Installation and Removal of Jack-up Units.* Joint Industry-funded Project, RPS Energy, U.K. http://www.cofs.uwa.edu.au/data/assets/pdf_file/0009/2466495/InSafeJIP_Guideline_Rev_1c_28Mar11.pdf

Osborne, J.J. and Paisley, J.M. (2002). "South East Asia jack-up punch-throughs: The way forward." *Proceedings of the International Conference on Offshore Site Investigation and Geotechnics — Sustainability and Diversity,* London, U.K., 301-306. https://www.onepetro.org/conference-paper/SUT-OSIG-02-301

Rad, N.S. and Tumay, M.T. (1987). "Factors affecting sand specimen preparation by raining." *Geotechnical Testing Journal,* **10**(1), 31-37. https://doi.org/10.1520/GTJ10136J

Society of Naval Architects and Marine Engineers (SNAME) (2008). *Guideline for Site Specific Assessment of Mobile Jack-Up Units.* Technical and Research Bulletin 5-5A, Jersey City, NJ, USA. https://www.proceedings.com/0131.html

Swancor (2017). "Green energy and environmental protection and safety." Nantou, Taiwan. https://www.swancor.com/tw/project.php?act=videolist

Taiwan Power Company (2009). *Geological and Bathymetric Investigation Report*. *Feasibility Study Changhua Offshore Wind Energy, Appendix II* (in Chinese).

Terzaghi, K. (1943). *Theoretical Soil Mechanics*. John Wiley and Sons, Hoboken, NJ, U.S.A. https://onlinelibrary.wiley.com/doi/book/10.1002/9780470172766

Vesic, A.S. (1967). *A Study of Bearing Capacity of Deep Foundations.* Final Report, Project B-119, Georgia Institute of Technology, Atlanta, U.S.A. https://trid.trb.org/view/119544

Young. A.G., Remmes, B.D., and Meyer, B.J. (1984). "Foundation performance of offshore jack-up drilling rigs." *Journal of Geotechnical Engineering*, ASCE, **110**(7), 841-859. https://doi.org/10.1061/(ASCE)0733-9410(1984)110:7(841)